Interaction of nickel ferrite nanoparticles with nucleic acids

Seda Nur Topkaya [a],[*], I. İdil Karaca Açarı [b], Hüseyin Oğuzhan Kaya [a], I. İmren Özcan [c], Süleyman Köytepe [c], Arif E. Cetin [d]

[a] *Department of Analytical Chemistry, Faculty of Pharmacy, Izmir Katip Celebi University, Izmir, Turkey*
[b] *Department of Bioengineering, Faculty of Engineering and Natural Sciences, Malatya Turgut Ozal University, Malatya, Turkey*
[c] *Department of Chemistry, Faculty of Science, Inonu University, Malatya, Turkey*
[d] *Izmir Biomedicine and Genome Center, Izmir, Turkey*

ARTICLE INFO

ABSTRACT

In this article, we introduced an electrochemical biosensor employing graphite electrodes (GE) decorated with Nickel ferrite ($NiFe_2O_4$) nanoparticles for nucleic acid detection. $NiFe_2O_4$ nanoparticles in a narrow size distribution were synthesized with co-precipitation technique. Their chemical and crystallographic properties were characterized with FTIR and X-ray spectroscopies. Nanoparticle size distribution and hydrodynamic diameter were determined with particle size analyzer. Elemental content and purity of nanoparticles were analyzed with EDX analysis. Our analyses showed a diameter of ~10 nm for $NiFe_2O_4$ nanoparticles. Electrochemical properties of $NiFe_2O_4$ nanoparticles were examined with different analysis methods. Conductivity properties of $NiFe_2O_4$ nanoparticles were investigated with Cyclic Voltammetry (CV), which confirmed that nanoparticles on GE surface have a high surface area and conductivity. More importantly, in this article, the interactions between $NiFe_2O_4$ nanoparticles and double stranded DNA (dsDNA), single stranded DNA (ssDNA), and RNA were for the first time examined using Differential Pulse Voltammetry (DPV), CV, and Electrochemical Impedance Spectroscopy (EIS). Oxidation peak currents of $NiFe_2O_4$ nanoparticles and guanine bases of dsDNA, ssDNA, and RNA showed that $NiFe_2O_4$ nanoparticles effectively interacts with nucleic acids via an electrostatic mode.

1. Introduction

Ferrites, composed of iron oxides and ferromagnetic compounds, could be chemically mixed with other metals. Ferrite based magnetic metal oxides such as Fe_3O_4, $CoFe_2O_4$, $NiFe_2O_4$, and $ZnFe_2O_4$ have great potential in catalyst [1], magnetic recording [2], controlled drug release [3–5], and photovoltaic cells [6,7] due to their unique electrical, magnetic and semiconductor properties [8]. Ferrites can also take place in medical practices as inter-body drug delivery [9], molecular imaging [10], and hyperthermia treatment [11] due to their biocompatibility, biodegradability, and chemical stability. Ferrites have a uniform particle size, and show a narrow size distribution. The nm-sized ferrites are in the formula of MFe_2O_4, which M corresponds to divalent fricative metal ions such as Ni, Zn, Co, Mn, and Cu. Among these nanoparticles, nickel ferrite ($NiFe_2O_4$), a soft ferrite material and one of the most important spinel ferrites, took significant attention as they have high frequency and electrical conductivity, permeability, mechanical and electrochemical stability, and resistance to corrosion [12]. $NiFe_2O_4$, n-type semiconductors, has an inverse spinel structure, and show typical ferri-

magnetic properties, less eddy current loss, high curie temperature, low magnetic anisotropy, and coercivity [13]. In their structure, there are ferric ions (Fe^{3+}) in the tetrahedral region, and a mixture of nickel (Ni^{2+}) with ferric ions (Fe^{3+}) in the ratio of 1:1 in the octahedral region.

Biosensors selectively detect biological molecules, and conjugate with their target on nanomaterial transducer, which converts this conjugation into a detectable and quantifiable signal. The transduction could be optical, mass sensitive, thermal or electrochemical. The use of $NiFe_2O_4$ nanoparticles within the biosensor applications has been preferred due to their excellent conductive feature [14–16], allowing the target molecules to bind easily to the surface of interest [17], quicker mass transfer [18], and eco-friendly nature. Magnetic and electrical properties of $NiFe_2O_4$ nanoparticles mostly rely on the synthesis methods such as sol-gel, hydrothermal, co-precipitation, chemical route, self-propagating, sonochemical, ball milling, microwave assisted sol-gel, and combustion [19]. Each of the aforementioned synthesis process has both advantages and disadvantages. In general, biosensor applications need smaller nanoparticles with a uniform shape for stable physio-

[*] Correspondence to: Izmir Katip Celebi University, Faculty of Pharmacy, Department of Analytical Chemistry, Izmir, Turkey.
E-mail address: sedanur6@gmail.com (S.N. Topkaya).

chemical properties so that method selection to obtain proper nanoparticle size and shape is critical. For all these synthesis methods, the co-precipitation allows to adjust the particle size and shape by controlling the precipitation reaction. Organic additives such as oleic acid or surface complexing agents such as dextran can be used during nanoparticle formation to control particle size distribution [20]. Particle size could be also adjusted by changing the solution composition, pH, reaction time, stirring, and temperature. In co-precipitation reactions, nucleation, growth, and agglomeration occur simultaneously. Despite these advantages, co-precipitation reactions cannot be performed to uncharged species, which limits its application. In addition, trace quantity of impurities could form alongside with the product during the precipitation reaction.

Nanomaterials have been used in biosensors and nucleic acid hybridization studies especially for small molecules and nucleic acid interaction. For instance, the interaction between isoproterenol and cardiomyocyte DNA was analyzed with glassy carbon electrodes using an electrochemical biosensor which incorporated carbon nanotubes, polyaniline, and gold nanoparticles to increase the conductivity and sensitivity [21]. In another study, the interaction of curcumin and DNA was detected with an electrochemical biosensor that consists of hydroxyapatite nanoparticles and ionic liquid modified pencil graphite electrodes. By evaluating the changes of the oxidation signals of curcumin and guanine bases of DNA, curcumin was found to change the DNA secondary structure [22]. As an example of hybridization study employing nanomaterials in biosensors, polyaniline polymer, samarium oxide nanoparticles, and reduced graphene oxide were used to modify working electrodes for detecting a gene which is related to the familial Amyotrophic lateral sclerosis (ALS) disease [23]. Moreover, Cajigas et al. detected Zika virus genetic material with gold nanoparticle and DNA-based nanobioconjugate. The nanobioconjugate formed by the single-stranded DNA with gold nanoparticles was found to be more stable than the gold nanoparticle alone [24].

In this article, $NiFe_2O_4$ nanoparticles with an average diameter of ~10 nm were prepared using the co-precipitation technique. Chemical, structural, morphological, and thermal properties of these particles were characterized, and their electrochemical properties were examined. Nanoparticles are generally used to improve the sensitivity of the designed biosensor by providing larger surface area and higher conductivity compared to unmodified surfaces, while their interaction with analytes are not investigated. To the best of our knowledge, this study is the first one using $NiFe_2O_4$ nanoparticles combined with graphite electrodes for the development of an electrochemical biosensor for the detection of nucleic acids. For the first time, the interaction of $NiFe_2O_4$ nanoparticles with double stranded DNA (dsDNA), single stranded DNA (ssDNA), and RNA were investigated electrochemically by monitoring the alterations in the intrinsic oxidation peak currents of $NiFe_2O_4$ nanoparticles. In addition, the changes within the oxidation peak current of guanine bases after the interaction between $NiFe_2O_4$ nanoparticles and dsDNA and ssDNA were evaluated. We used Differential Pulse Voltammetry (DPV), and Cyclic Voltammetry (CV) to examine the interaction mechanism, and confirmed our results with Electrochemical Impedance Spectroscopy (EIS).

2. Material and methods

2.1. Chemicals and buffers

$FeCl_3.6 H_2O$, $NiCl_2.6 H_2O$, Trizma HCI, and EDTA disodium salt dehydrate were obtained from Sigma-Aldrich. NH_3, NaOH, NaCl, K_2HPO_4, KH_2PO_4, $K_3[Fe(CN)_6]$, and $K_4[Fe(CN)_6]$ were obtained from Merck. Ethanol absolute (%99.9) and glacial acetic acid were obtained from Isolab Chemicals. Buffers used in the experiments are 0.5 M Acetate (ACB, pH: 4.8), 0.05 M Phosphate (PBS, pH: 7.4), 0.05 M Tris-EDTA (TE, pH: 8.0), and 0.1 M Tris (TBS, pH:8.7).

2.2. Oligonucleotides

dsDNA from fish sperm were obtained from Sigma-Aldrich. ssDNA and RNA were obtained from EUROFINS-MWG. In RNA sequences, inosine (I) bases were used instead of guanine (G). The base sequences are shown below:

ssDNA: 5′-TCG TAC CGT GAG TAA TAA TGC G-3′.
RNA: 5′-CIC ATT ATT ACT CAC IIT ACI A-3′.

Stock solutions of oligonucleotides (1 mg/mL) were prepared with TE and kept at − 20 ˚C.

2.3. Instrumentation

Chemical structure of synthesized $NiFe_2O_4$ nanoparticles was determined with Perkin Elmer Spectrum Two FTIR spectrometer. ATR technique was used in FTIR analyses, and measurements were performed in the range of 400–4000 cm^{-1} at a resolution of 4 cm^{-1}. Rigaku RadB-DMAX II diffractometer was used for X-ray analyses of magnetic nanoparticles at a sensitivity of 0.02 and in the range of 10–80 2-Theta. LEO EVO-40xVP scanning electron microscope (SEM) was used to examine the structural and morphological properties of $NiFe_2O_4$ nanoparticles. SEM images were taken at 2 kV acceleration voltage and 3 mm working distance. Before each measurement, samples were covered with Au-Pd conductive coating using a Baltec brand spatter. Elemental verification of nanoparticle structures was carried out using Bruker Xflash EDX detector connected to SEM. Malvern Zetasizer Nano ZS particle characterization system was used to measure hydrolytic size distribution of nanoparticle structures. Physical particle sizes have been provided with high magnification TEM (Hitachi HT7800) analyses. Shimadzu DTA-50 and Shimadzu TGA-50 thermal analyzers were employed for determining thermal properties of magnetic nanoparticles at 10 ˚C/min heating rate and in air atmosphere. All thermal analyses were carried out in platinum sample pan using approximately 10 mg of sample. Electrochemical measurements were conducted using AUTOLAB 204. FRA32M potentiostat/galvanostat/impedance analyzer with NOVA 2.1 software. Graphite electrodes (GE), a platinum wire, an Ag/AgCl electrode were employed as working, auxiliary, and reference electrodes, respectively. In order to hold to pencil lead (Tombo, Japan) bought from a local bookstore, Pencil T 0.5 (Rotring, Germany) was used.

2.4. Methods

2.4.1. Synthesis of magnetic $NiFe_2O_4$ nanoparticles

For synthesis of $NiFe_2O_4$ nanoparticles, 0.2 M 100 mL iron chloride hexahydrate ($FeCl_3.6 H_2O$) solution and 0.1 M 100 mL nickel (II) chloride hexahydrate ($NiCl_2.6 H_2O$) solution were mixed. pH was adjusted to be greater than 10 by dropping 1.5 M NaOH solution. Final solution was refluxed at 80 ˚C for 3 h.

After 3 h of stirring, solution color changed to black, and the precipitate was separated in a centrifuge at 5000 rpm for 10 min. Black $NiFe_2O_4$ nanoparticles were laved with distilled water and ethyl alcohol to distract excess reactive molecules, and dried at 100 ˚C for 2 h. We started the structural characterization after $NiFe_2O_4$ nanoparticles were calcined at approximately 600 ˚C for 4 h.

2.4.2. Activation of graphite electrodes

Prior to the modification, + 1.4 V was applied to the graphite electrodes for 30 s in ACB to obtain clean activated electrode surfaces.

2.4.3. Modification of graphite electrodes with $NiFe_2O_4$ nanoparticles

1.5 mg $NiFe_2O_4$ nanoparticles were dissolved in 2 mL ethanol and 2 mL ultrapure water under ultrasonic agitation, and diluted with ACB. 100 μL of the solution was transferred to the vials. Electrodes were dipped into $NiFe_2O_4$ solution, and left at 60 ˚C, 500 rpm for 10 min. The

electrodes were ten washed with ACB. Finally, $NiFe_2O_4$ nanoparticle-modified graphite electrodes were dried at 60 °C for 5 min

2.4.4. Interaction of $NiFe_2O_4$ nanoparticles with different nucleic acids

The electrodes were activated and modified with $NiFe_2O_4$ nanoparticles as explained in Sections 2.4.2 and 2.4.3. They are then interacted with 500 µg/mL dsDNA, 10 µg/mL ssDNA, and 10 µg/mL RNA prepared in ACB as schematically shown in Fig. 1. Bare and $NiFe_2O_4$ nanoparticle - modified electrodes were immersed in these solutions for 20 min. Finally, the electrodes were washed with ACB.

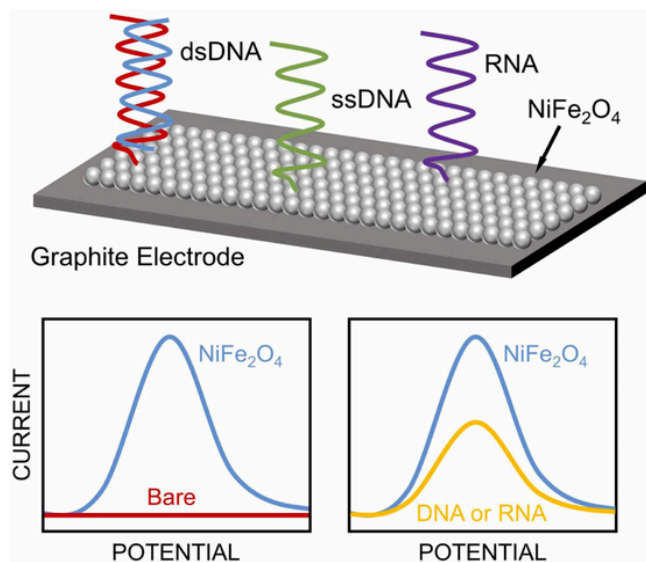**Fig. 1.** Schematic illustration of the interaction between $NiFe_2O_4$ nanoparticles and nucleic acids.

2.4.5. Measurement

DPV measurements were performed at 100 mV/s scan rate with 0.5 s interval time in ACB. CV measurements were performed in the range between - 0.05 V and + 0.6 V at 50 mV/s scan rate with 0.05 s interval time in 10 mM $K_{3/4}[Fe(CN)_6]$. EIS measurements were performed between 10^5 Hz and 0.1 Hz with 0.01 amplitude and 10 frequencies per decade in 10 mM $K_{3/4}[Fe(CN)_6]$.

3. Results and discussion

$NiFe_2O_4$ nanoparticles were analyzed with FTIR spectroscopy as shown in Fig. 2a. Here, two broad bands are seen between 357 and 476 cm^{-1} and 476–774 cm^{-1}. These two bands are associated with positive valence cations of the ferrite structure with tetrahedral and octahedral vibrations. Approximately 590 cm^{-1} corresponds to the internal stress vibrations of the metal in the tetrahedral region (Fe-O), while the band at approximately 410 cm^{-1} indicates octahedral (Ni-O) metal-oxygen stretching peak. Moreover, the band observed at ~1390 cm^{-1} is due to the stretching of H-O-H bond. The wide band observed between 3000 cm^{-1} and 3650 cm^{-1} shows the H-bond stress vibrations of the surface-OH groups of $NiFe_2O_4$ structure. The peak at ~3740 cm^{-1} is the O-H stretching vibration of H_2O structures absorbed on nanoparticle surface. Two small peaks observed at ~2950 cm^{-1} are due to the metal ion interaction on the particle surface.

Morphological properties of $NiFe_2O_4$ were examined with TEM (Fig. 2b). In these analyses, no reactive residues, impurity, and different phases were observed. Particular and highly porous structure of $NiFe_2O_4$ was observed especially at high magnifications. Using ImageJ program on TEM image (Fig. 2b), we determined a particle size of ~10 nm (Fig. S4). Fig. 2c shows the EDX spectrum, and Fig. 2d shows the elemental maps of $NiFe_2O_4$ nanoparticles. In the EDX spectrum, only Fe, Ni and O peaks were observed. For Fe; L_α, K_α and K_β peaks at 0.70, 6.44 and 7.04 keV values were detected. For Ni, peaks at 0.86,
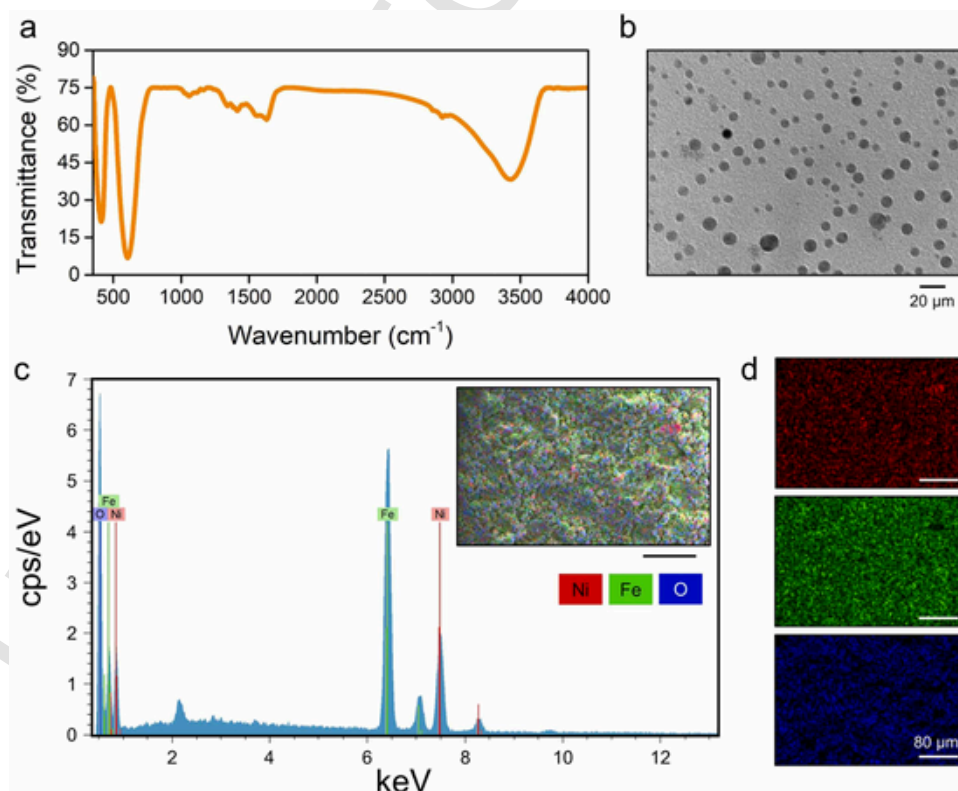

Fig. 2. (a) FTIR spectrum and (b) TEM image of $NiFe_2O_4$ nanoparticles. (c) EDX spectrum, (inset) EDX mapping, and (d) EDX elemental mapping of $NiFe_2O_4$ nanoparticles.

7.49 and 8.27 keV are associated with L_α, K_α and K_β. For the O, the distinct and clear peak at 0.51 keV is associated with K_α. EDX spectrum of $NiFe_2O_4$ nanoparticles confirmed the elemental purity of the prepared nanostructures, showing the homogeneous distribution of the synthesized $NiFe_2O_4$ nanoparticles. Furthermore, there is no significant aggregation between $NiFe_2O_4$ nanoparticle structures.

3.1. Electrochemical properties of $NiFe_2O_4$ nanoparticles

CV and DPV are preferred to understand the redox behavior of nanomaterials. In our study, electrochemical properties of $NiFe_2O_4$ nanoparticles were investigated with DPV (Fig. 3a and b), CV (Fig. 3c), and EIS (Fig. 3d). As shown in Fig. 3a, oxidation peak current of $NiFe_2O_4$ nanoparticles was detected at + 1.50 V with DPV. As shown in literature, electron exchange occurs between Ni^{2+}/Ni^+ and Fe^{2+}/Fe^{3+} in ferrites, and the oxidation results from $Fe^{2+} \rightarrow Fe^{3+} + e^-$ reaction [25]. In different studies, oxidation peak currents of $NiFe_2O_4$ nanoparticles were detected at + 0.3 V [13] and + 0.5 V [26].

Physical and chemical properties of nanoparticles depend on not only their size but also structure and surface coating. The reason behind the oxidation peak currents detected at different potentials in literature is the use of different working electrodes, e.g., we used pencil graphite electrodes, while glassy carbon electrodes were used elsewhere. Furthermore, synthesis method could also affect the location of the peak potential as we used a different technique compared to the other studies in literature. We also performed our measurements at a different pH value, which could also vary the oxidation peak current. Here, we chose pH as 4.8 as we achieved maximum adsorption of nucleic acids on the surface of nickel ferrite [27].

Stable immobilization of nanoparticles onto electrodes which provides stability and repeatability. In that sense, when the electrodes were dried in certain conditions, we could obtain more stable and repeatable signals. As shown in Figs. 3b and 3b-inset, higher oxidation

peak currents were provided with $NiFe_2O_4$ nanoparticle-modified electrodes dried at 60 °C for 5 min compared to non-dried $NiFe_2O_4$ nanoparticle-modified electrodes. After drying, oxidation peak currents of the modified electrodes increased by 93% compared to the non-dried electrodes. Relative standard deviation (RSD) was calculated as 11.3% and 2.8% for the non-dried and dried electrodes, respectively, which demonstrates dried electrodes' stability and repeatability.

Fig. 3c shows the Cyclic Voltammogram of $NiFe_2O_4$ nanoparticle-modified and bare electrodes in 10 mM $K_{3/4}[Fe(CN)_6]$ solution. Redox currents of $K_{3/4}[Fe(CN)_6]$ is higher for modified electrodes compared to bare ones due to their better electrical conductivity [28] as a result of easier electron exchange, i.e., the electrodes could be successfully coated with $NiFe_2O_4$ nanoparticles.

In order to calculate the electroactive surface area of $NiFe_2O_4$ nanoparticle-modified electrodes, Randless-Sevcik equation was used:

$$I_{pc} = (2\cdot69\times10^5)\ n^{3/2}\ D^{1/2}\ \nu^{1/2}\ A\ c \qquad \text{Eq. 1}$$

(Abbreviations in Eq. (1); I_{pc}: peak current, n: number of electrons, A: surface area of an electrode, D: diffusion coefficient, ν: scan rate, c: concentration).

According to Eq. (1), electroactive surface area of $NiFe_2O_4$ nanoparticle-modified electrodes 2.5 times larger compared to the bare electrodes, e.g., 25 mm² vs. 10 mm². In literature, electroactive surface area of MWCNT/$NiFe_2O_4$, reduced graphene oxide (rGO)/$NiFe_2O_4$ nanospheres, and nickel-zinc ferrite nanoparticles were found as 23 mm² [29], 24 mm² [30], and 18 mm² [31], respectively. Therefore, $NiFe_2O_4$ nanoparticles are sufficiently immobilized on the electrode surface, i.e., a suitable surface area was provided for further experiments.

We also used EIS to determine the interface properties of $NiFe_2O_4$ nanoparticle-modified and bare electrodes. Nyquist plots obtained from EIS could provide information about the charge-transfer resistance (R_{ct}), mass resistance, and capacitance between electrode and elec-
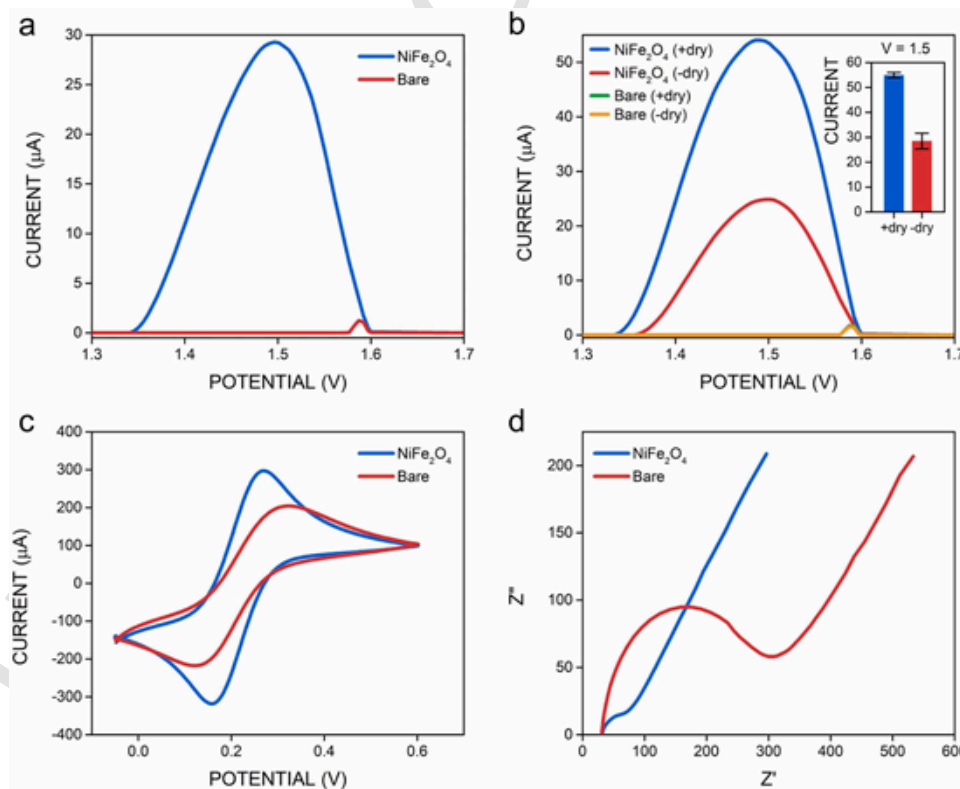
Fig. 3. (a) Differential Pulse Voltammogram for the oxidation peak currents of $NiFe_2O_4$ nanoparticle-modified and bare electrodes at + 1.5 V. **(b)** Differential Pulse Voltammogram for the oxidation peak currents of $NiFe_2O_4$ nanoparticle-modified and bare electrodes with/without drying at + 1.5 V. **(c)** Cyclic Voltammogram and **(d)** Electrochemical Impedance Spectra of $NiFe_2O_4$ nanoparticle-modified and bare electrodes in 10 mM $K_{3/4}[Fe(CN)_6]$ solution.

trolyte. Fig. 3d shows Nyquist plots that consists of two portions, e.g., a distorted semicircle in the high frequency range and the sloping straight line in a low frequency for the NiFe$_2$O$_4$ nanoparticle-modified and bare electrodes. For such type of impedance spectrum, semicircle refers to a limited transfer of electrons, where its diameter refers to the charge-transfer resistance value. In our study, we found that NiFe$_2$O$_4$ nanoparticle-modified and bare electrodes have average R$_{ct}$ values of 30 ± 4.5 Ω and 180 ± 12.6 Ω, respectively. The lower value of R$_{ct}$ for the modified electrodes is due to the swift charge transfer between electrolyte and electrode that verifies the well conductivity of the synthesized NiFe$_2$O$_4$ nanoparticles. As shown in literature, in ferrite nanoparticles, electron switch between cations of Ni^{2+}/Ni$^+$ and Fe^{2+}/Fe^{3+} provides conductivity [25].

We calculated the surface coverage (θ) of NiFe$_2$O$_4$ nanoparticles by using the following equation below [32]:

$$\theta = \left[1 - \frac{Rct \quad (coated)}{Rct \quad (bare)}\right] \times 100 \qquad \text{Eq. 2}$$

In the equation, R$_{ct}$(bare) and R$_{ct}$(coated) refer the charge-transfer resistance of the bare and NiFe$_2$O$_4$ nanoparticles coated electrodes, respectively. According to the equation above, the corresponding surface coverage of with NiFe$_2$O$_4$ nanoparticles was calculated as 83%, which shows the good coating of the electrodes.

Effect of scan rate (ν) on NiFe$_2$O$_4$ nanoparticle oxidation current (Ip$_a$) was examined with CV in 10 mM K$_{3/4}$[Fe(CN)$_6$] solution. The peak current increased with scan rate in the range between 20 and 150 mV/s (Fig. 4). The relationship between NiFe$_2$O$_4$ nanoparticle peak current (Ip$_a$) and scan rate (ν) has a linear behavior (Fig. 4a):

$$Ip_a\,(\mu A) = 0.002 \quad \nu \quad + \quad 2.2376 \quad (R^2 = 0.9953) \qquad \text{Eq. 3}$$

The relationship between NiFe$_2$O$_4$ nanoparticle peak current (Ip$_a$) and the root of the scan rate (ν$^{1/2}$) also possesses a linear behavior (Fig. 4b):

$$Ip_a\,(\mu A) = 20.136 \quad \nu^{1/2} + 87.899 \quad (R^2 = 0.9754) \qquad \text{Eq. 4}$$

The linear correlation among Ip$_a$ and ν$^{1/2}$ implies that the process is diffusion-controlled [33].

Such linear behavior was also determined between log(Ip$_a$) and log (ν) within the scan rate range between 20 mV/s and 150 mV/s (Fig. 4c):

$$\log Ip_a = \quad 0.256 \log \nu - 0.2135 \quad (R^2 = 0.9949) \qquad \text{Eq. 5}$$

3.2. Interaction of NiFe$_2$O$_4$ nanoparticles with nucleic acids

Important modes of DNA-small molecule interaction, such as drugs, chemicals or nanoparticles, include covalent or non-covalent (intercalation, groove binding and electrostatic) interactions. It is important to understand the interaction mode for the action mechanism of the particular molecule. In our study, the interaction between NiFe$_2$O$_4$ nanoparticles and nucleic acids, e.g., ssDNA, dsDNA, and RNA was examined with DPV and EIS. Interaction study consists of four main steps: (i) pre-treatment of the electrode surface for acquiring a more hydrophilic surface to favor nucleic acid immobilization, (ii) ssDNA, dsDNA, and RNA immobilization, (iii) interaction with NiFe$_2$O$_4$ nanoparticles and nucleic acid molecules, (iv) measurement of both oxidation peak currents of guanine and NiFe$_2$O$_4$ nanoparticles.

In Figs. 5a and 5a-inset, oxidation peak currents were evaluated, which belong to guanine (at +1.0 V) and NiFe$_2$O$_4$ nanoparticles (at +1.5 V) after the interaction with ssDNA. For ssDNA, the signals that belong to guanine bases decreased after the interaction with NiFe$_2$O$_4$ nanoparticles. Similar observation was valid for the oxidation peak currents of NiFe$_2$O$_4$ nanoparticles, e.g., decreasing after the interaction with ssDNA. Oxidation peak currents of guanine and NiFe$_2$O$_4$ nanoparticles decreased by 20% and 70% after the interaction with ssDNA. Moreover, oxidation peak potential of NiFe$_2$O$_4$ nanoparticles shifted to more negative values after the interaction with ssDNA, which is due to
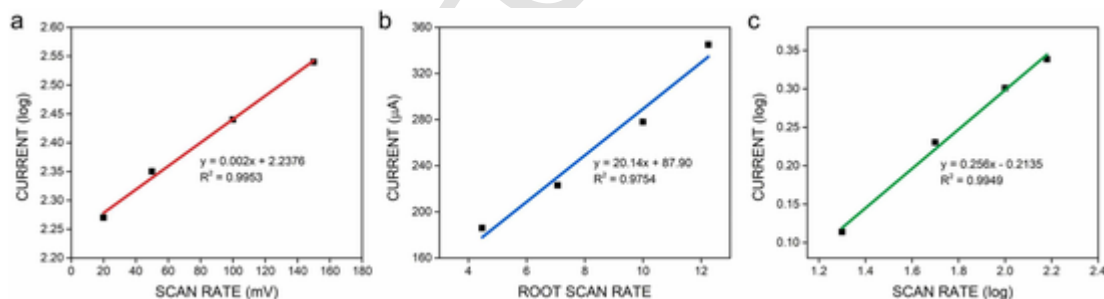

Fig. 4. (a) Effect of scan rate on peak current. **(b)** Effect of scan rate root on peak current. **(c)** Effect of scan rate on the log of peak current of NiFe$_2$O$_4$ nanoparticles.

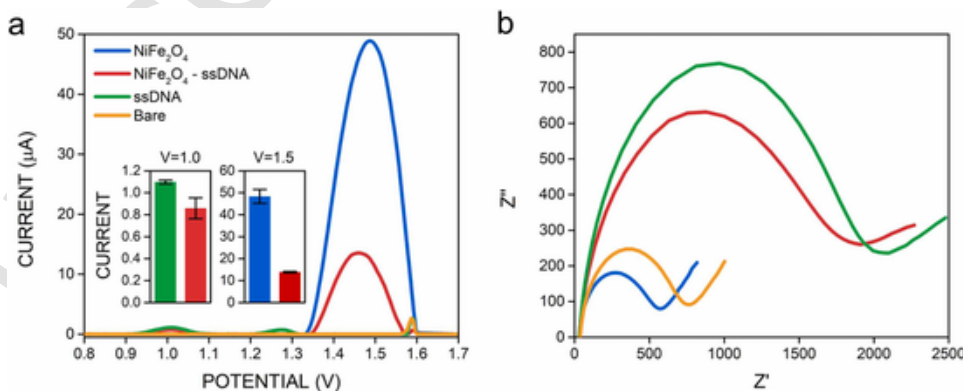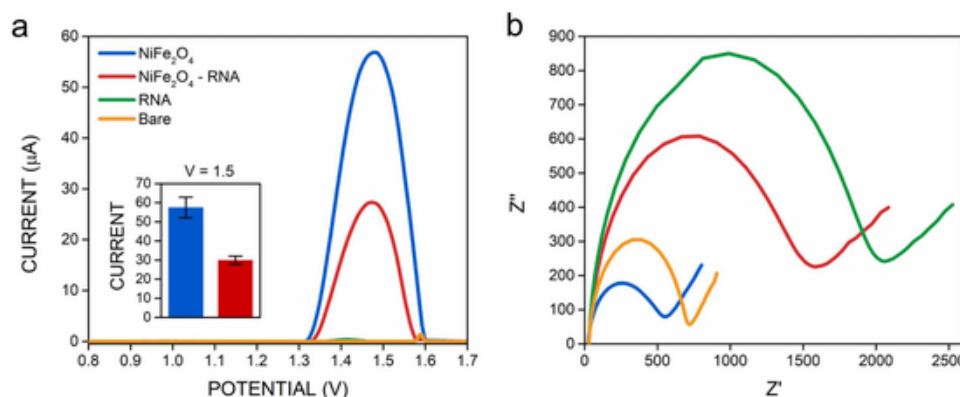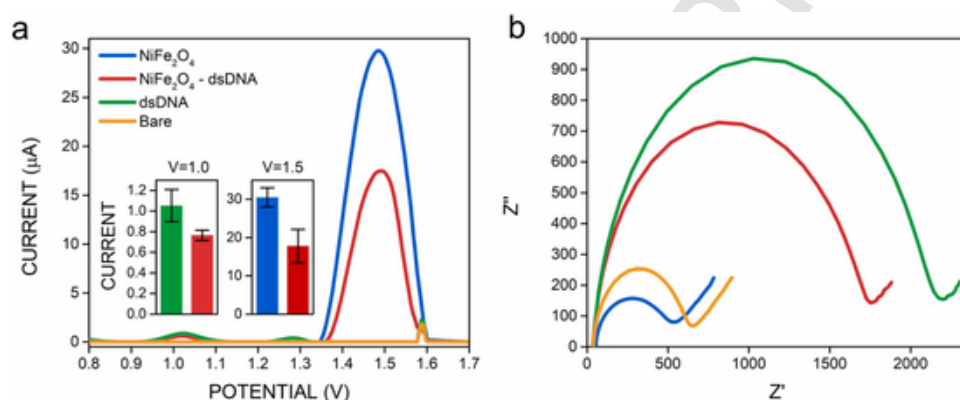

Fig. 5. (a) Differential Pulse Voltammogram, **(inset)** histogram for the oxidation peak currents of guanine bases of ssDNA (at + 1.0 V) and the NiFe$_2$O$_4$ nanoparticles (at + 1.5 V) before and after interaction with each other. (b) Electrochemical Impedance Spectra for bare, ssDNA coated, and NiFe$_2$O$_4$ nanoparticle-modified electrodes before and after interaction with each other.

Fig. 6. (a) Differential Pulse Voltammogram, and **(inset)** the histogram for the oxidation peak currents of NiFe$_2$O$_4$ nanoparticles (at $+1.5$ V) before and after the interaction with RNA. **(b)** Electrochemical Impedance Spectra for bare, RNA coated, and NiFe$_2$O$_4$ nanoparticle modified-electrodes before and after the interaction with each other.

Fig. 7. (a) Differential Pulse Voltammogram, and **(inset)** histogram for the oxidation peak currents of guanine bases of dsDNA (at $+1.0$ V) and NiFe$_2$O$_4$ nanoparticles (at $+1.5$ V) before and after interaction with each other. (b) Electrochemical Impedance Spectra for bare, dsDNA coated, and NiFe$_2$O$_4$ nanoparticle-modified electrodes before and after interaction with each other.

the interaction mechanism between molecule and ssDNA that could be electrostatic in nature [34]. On the other hand, when the peak potential shifts to more positive values, the interaction is through intercalation. If there is no change observed, the interaction of the reduced form of the molecule is identical as that of its oxidized form. It should be noted that two binding modes could be present at the same time, and a single compound could possibly interact with DNA with more than one binding fashion, e.g. intercalation and covalent binding [35].

Electrochemical investigation of the interaction between NiFe$_2$O$_4$ nanoparticles and ssDNA was examined with EIS by evaluating the change of R_{ct} before and after the immobilization of ssDNA onto the surface of bare and NiFe$_2$O$_4$ nanoparticle-modified electrodes (Fig. 5b). The average R_{ct} values were recorded as $150 \pm 8.6\,\Omega$ (NiFe$_2$O$_4$ nanoparticles), $250 \pm 14.5\,\Omega$ (bare), $615 \pm 21.4\,\Omega$ (NiFe$_2$O$_4$-ssDNA), and $735 \pm 9.8\,\Omega$ (ssDNA). After the interaction between NiFe$_2$O$_4$ nanoparticles and ssDNA, R_{ct} value decreased compared only to ssDNA-coated electrodes before the interaction. An increase in R_{ct} value was observed which is due to the negative charges coming from the phosphate backbone of the DNA, averting $[Fe(CN)6]^{3-/4-}$ from attaining the surface of the electrodes. The decrease in the R_{ct} value also clearly proves the interaction between NiFe$_2$O$_4$ nanoparticles and ssDNA. In Fig. 5b, EIS results confirm the DPV results (Fig. 5a).

As shown in Fig. 6a and a-inset, oxidation peak current of NiFe$_2$O$_4$ nanoparticles decreased nearly half after the interaction with RNA. The decrease in the oxidation signal of NiFe$_2$O$_4$ nanoparticles after the interaction with RNA was less than with ssDNA. We can conclude that ss-DNA binds to NiFe$_2$O$_4$ nanoparticles easier than RNA. Since guanine base is not present in the RNA sample, we obtained no guanine oxida-

tion signal. There was no shift for the peak potential of NiFe$_2$O$_4$ nanoparticles after the interaction with RNA. In Fig. 6b, the interaction between NiFe$_2$O$_4$ nanoparticles and RNA was examined with EIS. Average R_{ct} values were determined as $180 \pm 12.1\,\Omega$ (NiFe$_2$O$_4$ nanoparticles), $302 \pm 18.7\,\Omega$ (bare), $598 \pm 25.1\,\Omega$ (NiFe$_2$O$_4$-RNA), and $852 \pm 19.4\,\Omega$ (RNA). After the interaction between NiFe$_2$O$_4$ nanoparticles and RNA, R_{ct} value decreased compared only toRNA coated electrodes before the interaction.

As shown in Fig. 7a and a-inset, after the interaction with dsDNA, oxidation peak currents of guanine and NiFe$_2$O$_4$ nanoparticles (at $+1.5$ V) decreased by 20% and 40%, respectively. Here, ssDNA binds to the nanoparticles easier than dsDNA similar to RNA. Peak potential of NiFe$_2$O$_4$ nanoparticles shifted to more negative values after the interaction with dsDNA. In Fig. 7b, the interaction between NiFe$_2$O$_4$ nanoparticles and dsDNA was studied with EIS, where the average R_{ct} values were found as $163 \pm 8.2\,\Omega$ (NiFe$_2$O$_4$ nanoparticles), $254 \pm 13.6\,\Omega$ (bare), $718 \pm 13.9\,\Omega$ (NiFe$_2$O$_4$-dsDNA), and $936 \pm 25.8\,\Omega$ (dsDNA).

Small molecules like drugs-DNA interactions can be listed in four different binding types, e.g., electrostatic binding, groove binding, external binding, and intercalative binding. For instance, the interaction of Diclofenac and DNA was analyzed by evaluating the oxidation peak currents of guanine bases of DNA and the shift of the peak potential. The peak potential shifted to more positive values which indicated the intercalation [36]. In literature, the isoelectric point of NiFe$_2$O$_4$ nanoparticles was found at pH of 7.7 [27]. Below this pH value, NiFe$_2$O$_4$ nanoparticles is positively charged because of high concentration H^+ ions. Above this pH value, NiFe$_2$O$_4$ nanoparticles is negatively

charged because of high concentration OH$^-$ ions. In our study, we performed the interaction studies at pH of 4.8. According to literature, this pH is below than the isoelectric point of NiFe$_2$O$_4$ nanoparticles. Thus, NiFe$_2$O$_4$ nanoparticles is positively charged at this pH. In addition, DNA is negatively charged because of its phosphate groups with negatively charged. Nucleic acids could be physically conjugated to nanoparticles with electrostatic, van der Waals and other weak forces. Analyzing the interaction with ssDNA, dsDNA, and RNA, we could conclude that interaction of NiFe$_2$O$_4$ nanoparticles with nucleic acids could be ensured by coordination bonds among cobalt and iron ions at the particle surface with oxygen atoms of PO$_2^-$ groups of a sugar-phosphate frame and C$=$O groups of nucleic base heterocycles [37]. Interaction between ssDNA/dsDNA/RNA and NiFe$_2$O$_4$ nanoparticles could be electrostatic, which could most likely involved in positive sites of metal ferrite and negative sites (PO$_3^{2-}$ group) of nucleic acid constituents [27]. All these findings prove that there is an electrostatic interaction between positively charged NiFe$_2$O$_4$ nanoparticles and negatively charged nucleic acids at a pH level below the isoelectric point.

4. Conclusion

In this study, NiFe$_2$O$_4$ nanoparticles were synthesized in a narrow size distribution with co-precipitation technique. We showed that the electroactive surface area of NiFe$_2$O$_4$ nanoparticle-coated working electrodes increased by 2.5 folds compared to non-coated ones. Considering the changes in the oxidation signals of NiFe2O4 nanoparticles, it is clear that interaction occurs between the nanoparticles and nucleic acids. When the rate of changes in the oxidation signals of the nanoparticles is examined, it is seen that there is a clear difference between the interaction of nanoparticles with ssDNA and dsDNA, while it interacts more with ssDNA. Oxidation peak potential of NiFe$_2$O$_4$ nanoparticles shifted to more negative values after the interaction with ssDNA and dsDNA. We believe our findings could play an important role in the context of prebiotic chemistry for the interaction of spinel metals and nucleic acids. Furthermore, NiFe$_2$O$_4$ nanoparticles could be used as an electrochemical hybridization indicator due to its unique electrochemical behavior to nucleic acids.

Conflict of interest

None.

CRediT authorship contribution statement

Seda Nur Topkaya: Conceptualization, Methodology, Investigation, Formal analysis, Writing – review & editing, Supervision. **İdil Karaca Açarı:** Methodology, Investigation, Formal analysis, Writing – review & editing. **Hüseyin Oğuzhan Kaya:** Investigation, Formal analysis, Writing – review & editing. **İmren Özcan:** Investigation, Formal analysis. **Süleyman Köytepe:** Methodology, Formal analysis. **Arif E. Cetin:** Conceptualization, Methodology, Formal analysis, Writing – review & editing.

Declaration of Competing Interest

The authors declare that they have no known competing financial interests or personal relationships that could have appeared to influence the work reported in this paper.

Appendix A. Supporting information

Supplementary data associated with this article can be found in the online version at doi:10.1016/j.colsurfb.2021.112282.

References

[1] K. Kombaiah, J.J. Vijaya, L.J. Kennedy, K. Kaviyarasu, Catalytic studies of NiFe2O4 nanoparticles prepared by conventional and microwave combustion method, Mater. Chem. Phys. 221 (2019) 11–28.

[2] S.P. Pernal, A.J. Willis, M.E. Sabo, L.M. Moore, S.T. Olson, S.C. Morris, F.M. Creighton, H.H. Engelhard, An in vitro model system for evaluating remote magnetic nanoparticle movement and fibrinolysis, Int. J. Nanomed. 15 (2020) 1549–1568.

[3] Y. Fang, S. Lin, F. Yang, J. Situ, S. Lin, Y. Luo, Aptamer-conjugated multifunctional polymeric nanoparticles as cancer-targeted, mri-ultrasensitive drug delivery systems for treatment of castration-resistant prostate cancer, BioMed. Res. Int. 2020 (2020) 9186583.

[4] P. Parlanti, A. Boni, G. Signore, M. Santi, Targeted dendrimer-coated magnetic nanoparticles for selective delivery of therapeutics in living cells, Molecules 25 (2020).

[5] P. Dwivedi, S. Kiran, S. Han, M. Dwivedi, R. Khatik, R. Fan, F.A. Mangrio, K. Du, Z. Zhu, C. Yang, F. Huang, A. Ejaz, R. Han, T. Si, R.X. Xu, Magnetic targeting and ultrasound activation of liposome-microbubble conjugate for enhanced delivery of anticancer therapies, ACS Appl. Mater. Interfaces 12 (2020) 23737–23751.

[6] N. Abraham, A. Rufus, C. Unni, D. Philip, Dye sensitized solar cells using catalytically active CuO-ZnO nanocomposite synthesized by single step method, Spectrochim. Acta Part A, Mol. Biomol. Spectrosc. 200 (2018) 116–126.

[7] M. Klein, R. Pankiewicz, M. Zalas, W. Stampor, Magnetic field effects in dye-sensitized solar cells controlled by different cell architecture, Sci. Rep. 6 (2016) 30077.

[8] E. Tanrıkut, İ. Özcan, E. Sel, S. Köytepe, E.K. Savan, Simultaneous electrochemical detection of estradiol and testosterone using nickel ferrite oxide doped mesoporous carbon nanocomposite modified sensor, J. Electrochem. Soc. 167 (2020) 087509.

[9] K. Yang, G. Yu, R. Tian, Z. Zhou, H. Deng, L. Li, Z. Yang, G. Zhang, D. Liu, J. Wei, L. Yue, R. Wang, X. Chen, Oxygen-evolving manganese ferrite nanovesicles for hypoxia-responsive drug delivery and enhanced cancer chemoimmunotherapy, Adv. Funct. Mater. 31 (2021) 2008078.

[10] M. Pernia Leal, S. Rivera-Fernández, J.M. Franco, D. Pozo, J.M. de la Fuente, M.L. García-Martín, Long-circulating PEGylated manganese ferrite nanoparticles for MRI-based molecular imaging, Nanoscale 7 (2015) 2050–2059.

[11] J. Sánchez, M. Rodríguez-Reyes, D.A. Cortés-Hernández, C.A. Ávila-Orta, P.Y. Reyes-Rodríguez, Heating capacity and biocompatibility of Pluronic-coated manganese gallium ferrites for magnetic hyperthermia treatment, Colloids Surf. A: Physicochem. Eng. Asp. 612 (2021) 125986.

[12] F. Majid, J. Rauf, S. Ata, I. Bibi, A. Malik, S.M. Ibrahim, A. Ali, M. Iqbal, Synthesis and characterization of NiFe2O4 ferrite: Sol–gel and hydrothermal synthesis routes effect on magnetic, structural and dielectric characteristics, Mater. Chem. Phys. 258 (2021) 123888.

[13] A.K.H. Bashir, N. Matinise, J. Sackey, K. Kaviyarasu, I.G. Madiba, L. Kodseti, F.I. Ezema, M. Maaza, Investigation of electrochemical performance, optical and magnetic properties of NiFe2O4 nanoparticles prepared by a green chemistry method, Phys. E: Low. -Dimens. Syst. Nanostruct. 119 (2020) 114002.

[14] H. BEITOLLAHI, S. TAJIK, M.R. AFLATOONIAN, A. MAKAREM, NiFe2O4 nanoparticles modified screen printed electrode for simultaneous determination of serotonin and norepinephrine, Anal. Bioanal. Electrochem. 10 (2018).

[15] M. Nouri, M. Rahimnejad, G. Najafpour, A.A. Moghadamnia, Simultaneous voltammetric determination of rizatriptan and acetaminophen using a carbon paste electrode modified with NiFe2O4 nanoparticles, Microchim. Acta 187 (2020) 315.

[16] T. Zabihpour, Voltammetric food analytical sensor for determining vanillin based on amplified NiFe2O4 nanoparticle/ionic liquid sensor, J. Food Meas. Charact. v. 14 (2020) 1039–1045, 2020 v.1014 no.1032.

[17] R. Devi, S. Gogoi, H.S. Dutta, M. Bordoloi, S.K. Sanghi, R. Khan, Au/NiFe2O4 nanoparticle-decorated graphene oxide nanosheets for electrochemical immunosensing of amyloid beta peptide, Nanoscale Adv. 2 (2020) 239–248.

[18] G. Kesavan, N. Nataraj, S.-M. Chen, L.-H. Lin, Hydrothermal synthesis of NiFe2O4 nanoparticles as an efficient electrocatalyst for the electrochemical detection of bisphenol A, N. J. Chem. 44 (2020) 7698–7707.

[19] M. Imran Din, F. Rafique, M.S. Hussain, H. Arslan Mehmood, S. Waseem, Recent developments in the synthesis and stability of metal ferrite nanoparticles, Sci. Prog. 102 (2019) 61–72.

[20] S. Laurent, D. Forge, M. Port, A. Roch, C. Robic, L. Vander Elst, R.N. Muller, Magnetic iron oxide nanoparticles: synthesis, stabilization, vectorization, physicochemical characterizations, and biological applications, Chem. Rev. 108 (2008) 2064–2110.

[21] J. Wang, Y. Li, C. Li, X. Zeng, W. Tang, X. Chen, A voltammetric study on the interaction between isoproterenol and cardiomyocyte DNA by using a glassy carbon electrode modified with carbon nanotubes, polyaniline and gold nanoparticles, Microchim Acta 184 (2017) 2999–3006.

[22] M. Uca, E. Eksin, Y. Erac, A. Erdem, Electrochemical investigation of curcumin–DNA interaction by using hydroxyapatite nanoparticles–ionic liquids based composite electrodes, Materials (Basel) 14 (2021) 4344.

[23] N. Mohammadian, F. Faridbod, ALS genosensing using DNA-hybridization electrochemical biosensor based on label-free immobilization of ssDNA on Sm2O3 NPs-rGO/PANI composite, Sens. Actuators B: Chem. 275 (2018) 432–438.

[24] S. Cajigas, D. Alzate, J. Orozco, Gold nanoparticle/DNA-based nanobioconjugate for electrochemical detection of Zika virus, Microchim Acta 187 (2020) 594.

[25] M.A.S. Amulya, H.P. Nagaswarupa, M.R.A. Kumar, C.R. Ravikumar, S.C. Prashantha, K.B. Kusuma, Sonochemical synthesis of NiFe2O4 nanoparticles:

Characterization and their photocatalytic and electrochemical applications, Appl. Surf. Sci. Adv. 1 (2020) 100023.

[26] M.E. Uddin, N.H. Kim, T. Kuila, S.H. Lee, D. Hui, J.H. Lee, Preparation of reduced graphene oxide-NiFe2O4 nanocomposites for the electrocatalytic oxidation of hydrazine, Compos. Part B: Eng. 79 (2015) 649–659.

[27] M.A. Iqubal, R. Sharma, Kamaluddin, Surface interaction of ribonucleic acid constituents with spinel ferrite nanoparticles: a prebiotic chemistry experiment, RSC Adv. 6 (2016) 68574–68583.

[28] I. Tiwari, M. Singh, C.M. Pandey, G. Sumana, Electrochemical detection of a pathogenic Escherichia coli specific DNA sequence based on a graphene oxide–chitosan composite decorated with nickel ferrite nanoparticles, RSC Adv. 5 (2015) 67115–67124.

[29] A.A. Ensafi, B. Saeid, B. Rezaei, A.R. Allafchian, Differential pulse voltammetric determination of methyldopa using MWCNTs modified glassy carbon decorated with NiFe2O4 nanoparticles, Ionics 21 (2015) 1435–1444.

[30] M.M. El-Wekil, A.M. Mahmoud, S.A. Alkahtani, A.A. Marzouk, R. Ali, A facile synthesis of 3D NiFe(2)O(4) nanospheres anchored on a novel ionic liquid modified reduced graphene oxide for electrochemical sensing of ledipasvir: Application to human pharmacokinetic study, Biosens. Bioelectron. 109 (2018) 164–170.

[31] A. Yarahmadi, T. Madrakian, A. Afkhami, N.R. Jalal, Electrochemical Determination of Sunitinib in Biological Samples Using Polyacrylonitrile Nanofibers/Nickel-Zinc-Ferrite Nanocomposite/Carbon Paste Electrode, J. Electrochem. Soc. 166 (2019) B1268–B1275.

[32] E. Sabatani, I. Rubinstein, R. Maoz, J. Sagiv, Organized Self-Assembling Monolayers on Electrodes.1. Octadecyl Derivatives on Gold, J. Electro Chem. 219 (1987) 365–371.

[33] N.P. Shetti, S.J. Malode, D. Ilager, K. Raghava Reddy, S.S. Shukla, T.M. Aminabhavi, A. Novel, Novel electrochemical sensor for detection of molinate using ZnO nanoparticles loaded carbon electrode, Electroanalysis 31 (2019) 1040–1049.

[34] S.D. Shahida Parveen, A. Affrose, B. Suresh Kumar, J. Annaraj, K. Pitchumani, Synthesis, Characterization, and DNA Binding Studies of Nanoplumbagin, J. Nanomater. 2014 (2014) 179149.

[35] M. Lazou, A. Tarushi, P. Gritzapis, G. Psomas, Transition metal complexes with a novel guanine-based (E)-2-(2-(pyridin-2-ylmethylene)hydrazinyl)quinazolin-4 (3H)-one: Synthesis, characterization, interaction with DNA and albumins and antioxidant activity, J. Inorg. Biochem. 206 (2020) 111019.

[36] L. Wei, J. Borowiec, L. Zhu, J. Zhang, Electrochemical investigation on the interaction of diclofenac with DNA and its application to the construction of a graphene-based biosensor, J. Solid State Electrochem. 16 (2012) 3817–3823.

[37] A.G. Pershina, A.E. Sazonov, D.V. Novikov, A.S. Knyazev, T.I. Izaak, V.I. Itin, E.P. Naiden, A.A. Magaeva, O.G. Terechova, Study of DNA interaction with cobalt ferrite nanoparticles, J. Nanosci. Nanotechnol. 11 (2011) 2673–2677.